SLEEPJ, 2019, 1–13

doi: 10.1093/sleep/zsz170
Advance Access Publication Date: 29 July 2019
Original Article

ORIGINAL ARTICLE

Infraslow coordination of slow wave activity through altered neuronal synchrony

Michael B. Dash[1,2,*]

[1]Department of Psychology, Middlebury College, Middlebury, VT and [2]Program in Neuroscience, Middlebury College, Middlebury, VT

*Corresponding author. Michael B. Dash, Department of Psychology, 281 McCardell Bicentennial Hall, 276 Bicentennial Way, Middlebury College, Middlebury, VT 05753. Email: mdash@middlebury.edu.

Abstract

Slow wave activity (SWA; the EEG power between 0.5 and 4 Hz during non-rapid eye movement sleep [NREM]) is the best electrophysiological marker of sleep need; SWA dissipates across the night and increases following sleep deprivation. In addition to these well-documented homeostatic SWA trends, SWA exhibits extensive variability across shorter timescales (seconds to minutes) and between local cortical regions. The physiological underpinnings of SWA variability, however, remain poorly characterized. In male Sprague-Dawley rats, we observed that SWA exhibits pronounced infraslow fluctuations (~40- to 120-s periods) that are coordinated across disparate cortical locations. Peaks in SWA across infraslow cycles were associated with increased slope, amplitude, and duration of individual slow waves and a reduction in the total number of waves and proportion of multipeak waves. Using a freely available data set comprised of extracellular unit recordings during consolidated NREM episodes in male Long-Evans rats, we further show that infraslow SWA does not appear to arise as a consequence of firing rate modulation of putative excitatory or inhibitory neurons. Instead, infraslow SWA was associated with alterations in neuronal synchrony surrounding "On"/"Off" periods and changes in the number and duration of "Off" periods. Collectively, these data provide a mechanism by which SWA can be coordinated across disparate cortical locations and thereby connect local and global expression of this patterned neuronal activity. In doing so, infraslow SWA may contribute to the regulation of cortical circuits during sleep and thereby play a critical role in sleep function.

Statement of Significance

Patterns of neuronal communication during sleep differ dramatically from the waking brain and appear to be causally related to sleep function. For example, cortical slow wave activity (SWA) appears critical for sleep-associated memory improvements. We provide a novel characterization of how infraslow fluctuations (~40- to 120-s cycles) coordinate the expression of SWA across disparate cortical locations. We further demonstrate that changes in SWA across infraslow cycles arise from changes in neuronal synchrony, rather than changes in firing rates. Understanding how neuronal activity during sleep is regulated provides a foundation for understanding both healthy sleep function and sleep pathology.

Key words: slow wave activity; infraslow; sleep regulation; neuronal synchrony; rat

Submitted: 19 February, 2019; **Revised:** 29 April, 2019

Introduction

Cortical slow wave activity (SWA; the EEG power between 0.5 and 4 Hz) is the best established electrophysiological marker of sleep need [1], exhibiting a canonical homeostatic decline across periods of prolonged sleep. In addition to its well-characterized homeostatic decline, however, SWA also exhibits extensive spatial and temporal variability. Given that the expression of SWA is important for sleep function [2–4], it is critical to understand the physiological mechanisms responsible for the coordination and regulation of SWA.

Individual slow waves originate within local cortical circuits and typically propagate through synaptic connections to generate a global slow wave [5, 6]. Propagation failures can result in the absence of slow waves within a local cortical circuit despite the presence of a slow wave elsewhere [7, 8], while the convergence of independently generated local slow waves may give rise to multipeak waves [9, 10]. Individual slow wave amplitudes vary considerably in conjunction with changes in the degree of neuronal synchronization [11]. Moreover, there appear to be distinct types of slow waves; local slow waves that are largely dependent upon corticocortical synchronization and global slow waves that may arise from subcorticocortical synchronization [12]. Each slow wave, therefore, represents a unique spatiotemporal sequence of neuronal activation and silence that depends upon both local and global regulators.

Like individual slow waves, SWA also exhibits widespread variability. SWA decreases along the anterior-posterior axis [13, 14] and changes locally as a consequence of previous waking activity [15–19]. Extensive variability in SWA across multiple timescales (e.g. years [20], hours [21], and minutes/seconds [22, 23]) further characterizes this dynamic process. The complex spatiotemporal expression of SWA can potentially lead to different functional outcomes; slow waves preferentially downscale weak synapses while preserving synaptic strength of neurons within active ensembles [24, 25]. Consequently, to fully characterize the functional consequences of sleep, it is critical to understand how the timing and expression of SWA is coordinated across cortical networks.

Infraslow fluctuations (<0.1 Hz) have previously been shown to modulate the power of higher frequency cortical activity during both sleep and wake states [22, 23, 26]. Moreover, these very slow fluctuations afford a powerful mechanism by which neuronal activity can be synchronized across disparate cortical regions [27–29]. For the present report, we investigated how infraslow activity modulates SWA expression. We observe that infraslow fluctuations are a significant source of SWA variability and coordinate SWA expression across two heterotypic, contralateral cortical regions (the right motor cortex and left parietal cortex). By examining neuronal firing rates and patterns across infraslow SWA cycles, we further show that changes in neuronal synchrony, rather than changes in neuronal firing rate, are associated with altered SWA across infraslow timescales.

Methods

The present study relies upon two distinct data sets: (1) chronic recordings of the electroencephalogram (EEG) and local field potential (LFP) recordings across the sleep/wake cycle in freely behaving male Sprague-Dawley rats (N = 7) and (2) LFP and neuronal spiking data recorded from frontal cortices during periods of consolidated sleep (at least 20-min episodes) and wake in male Long-Evans rats (N = 10). The first data set was recorded at Middlebury College, while the second was obtained from CRCNS.org [30], an online repository of freely available data. CRCNS.org data used this study were originally collected to address a different series of research questions [31].

Chronic EEG/LFP recordings in Sprague-Dawley rats

Stereotactic surgery.

Three- to four-month-old, male Sprague-Dawley rats (n = 7, Charles River; Wilmington, MA) were housed individually under standard laboratory conditions (12-h light/dark cycle, access to food and water ad libitum). To prepare for stereotactic surgery, rats were given a subcutaneous preoperative analgesic (Meloxicam; 2 mg/kg; MWI, Boise, ID), an intramuscular preoperative antibiotic (Penicillin; 100,000 units/kg), and isoflurane anesthesia (3.5% induction, 2%–3% maintenance). An LFP (0.003″ bare diameter Teflon-coated stainless steel wire, A-M Systems, Sequim, WA) was implanted into the right motor cortex (anterior-posterior [AP]: +2.0 mm, medial-lateral [ML]: +3.0 mm, dorsal-ventral [DV]: –1.5 mm). A second wire was affixed to a screw above the left parietal cortex (approximate AP: –4.0 mm, DV: –4.3 mm) and served as an electroencephalogram (EEG). Two additional stainless steel wires were affixed to screws above the cerebellum and served as a reference for the LFP/EEG leads and as a ground. To record the electromyogram (EMG), two braided stainless steel wires were inserted under the nuchal muscles. Two additional screws were attached to the skull to serve as anchors. All wires were connected to a headmount (8239 2EEG/1EMG Rat Headmount, Pinnacle Technologies, Lawrence, KS), and affixed in place with dental acrylic (Lang Dental, Wheeling, IL). One day post-surgery, each rat received a postoperative analgesic (Meloxicam; 2 mg/kg). These methods were carried out in accordance with the National Institutes of Health Guide for the Care and Use of Laboratory Animals and were approved by Middlebury College's Institutional Animal Care and Use Committee.

Data collection, processing, and analyses.

Rats were allowed a minimum of seven complete days to recover following surgery before continuous EEG/LFP/EMG recordings began. A flexible preamplifier (100× amplification, EEG/LFP high pass filter: 0.5 Hz, EMG high pass filter: 10 Hz; Pinnacle Technologies) was attached to both the rat's headmount and a commutator (SL6C, Plastics One, Roanoke, VA) to pass electrical signals into the data acquisition system (8401 DACS, Pinnacle Technologies) and enable unobstructed movement throughout the home cage. For each rat, data were continuously recorded (250 Hz; Sirenia Acquisition, Pinnacle Technologies) across a complete 24-h light/dark cycle. Behavioral state was determined offline through manual classification of LFP/EEG/EMG signals. Waking (high-frequency, low-voltage LFP/EEG activity coupled with EMG activity), non-rapid eye movement (NREM) sleep (low-frequency, high-voltage LFP/EEG activity absent EMG activity), and REM sleep (high-frequency, low-voltage LFP/EEG activity absent EMG activity) epochs were scored in 4-s epochs and vigilance state could be resolved for all epochs.

To process electrophysiological data, all EEG/LFP/EMG signals were first imported into Mathworks MATLAB (Natick, MA)

and subsequently analyzed using custom scripts. As a measure of sleep need [1], we calculated SWA from the power spectra (Welch's method, hamming window) by summing EEG or LFP power between 0.5 and 4 Hz. Average SWA was calculated in 30-min bins across the light period to examine the canonical homeostatic decline in SWA. Similar to previous reports [10, 32], to examine the underlying characteristics of individual slow waves that can contribute to SWA, EEG/LFP signals were band-pass filtered in the delta frequency range (0.5–4.0 Hz) with a zero-phase Chebyshev Type II filter. Local maxima during NREM sleep in these filtered tracings were used to identify individual slow waves. Maxima within 200 ms were considered part of the same individual slow wave (i.e. multipeak waves) while maxima separated by greater than 200 ms were considered unique individual slow waves. The amplitude, slope, and the number of peaks were quantified for each individual slow wave.

Much of the analyses of the present work focused on infraslow fluctuations in SWA. We first identified all consolidated NREM episodes (min duration 168 s, absent any visually scored brief arousals or REM sleep attempts). SWA across each consolidated NREM episode was then filtered in the infraslow range (zero-phase Chebyshev Type II filter, band pass: 0.004–0.025 Hz). From these filtered signals, instantaneous phase was calculated from the angle of the complex vector obtained from the Hilbert transform [23, 33]. Instantaneous phase data were primarily used for two sets of analyses: (1) examining the coordination of SWA across motor and parietal cortices and (2) examining the relationship between characteristics of individual slow waves and infraslow SWA phase.

To compare infraslow SWA phase across the motor and parietal cortices, instantaneous phase differences (IPD) were calculated ($IPD = e^{(i * (P_1 - P_2))}$), in which P_1 and P_2 are the instantaneous phase of the motor and parietal cortices, respectively. The average phase difference for that NREM episode was obtained from the imaginary component of the resultant complex number. To explore whether these infraslow phase differences are consistent across NREM episodes and rats, the infraslow cycle was first split into eight nonoverlapping phase bins. For each NREM episode, the percent of time that the motor cortex and parietal cortex exhibited an instantaneous phase difference within each of these bins was calculated. The percentages were then averaged across all NREM episodes and across all rats.

To further explore the relationships between infraslow SWA in the motor and parietal cortex, another set of analyses were conducted in the time domain. The cross-correlation (max lag: 150 s) between infraslow SWA in motor and parietal cortices was calculated for each NREM episode. Resultant cross-correlograms were averaged across NREM episodes and rats. To determine whether the average cross-correlogram was likely to have arisen by chance alone, a similar approach was taken except motor and parietal cortex infraslow episodes were randomly shuffled (1,000 times for each rat) prior to calculating the cross-correlation. From this bootstrap approach, a confidence interval depicting a cross-correlogram expected by chance alone was generated and served as the comparison distribution for the observed unshuffled cross-correlogram.

To investigate the relationships between infraslow SWA and infraslow fluctuations in different frequency bands, we first calculated band-limited power (BLP) for each 4-s epoch across a range of frequencies (SWA/delta: 0.5–4 Hz; theta: 6–9 Hz; alpha: 10–14 Hz; low_beta: 16–20 Hz; high_beta: 21–30 Hz; low_gamma: 40–59 Hz; and high_gamma: 61–80 Hz). Within each rat, the instantaneous phase of infraslow SWA (see above) was used to generate eight nonoverlapping phase bins that encompass the entire infraslow cycle. For each consolidated NREM episode, BLP values were normalized to the mean BLP of that NREM episode and averaged within each phase bin. Average infraslow BLP values were then correlated with average infraslow SWA.

Coupled LFP/neuronal spiking recordings in Long-Evans rats

To investigate potential physiological mechanisms that underlie infraslow SWA, a freely available data set was used (for full methodological details, see refs. [30, 31]). Briefly, this data set consists of continuous LFP and neuronal spiking activity recorded from deep cortical layers in frontal regions (Anterior Cingulate, Premotor, Medial Prefrontal, or Orbitofrontal Cortex) across consolidated episodes of sleep and wake in Long-Evans rats ($N = 11$). In the current report, a single animal's data from the original data set could not be loaded and therefore results are presented with an $N = 10$. In addition to LFPs and spiking data from putative excitatory and inhibitory neurons, this data set includes scored behavioral state and time stamps that identify the presence of "On" and "Off" firing periods during NREM sleep.

Firing rates and infraslow SWA.

A single, cortical LFP channel (identified in the original work [31] as a clean, artifact free signal) was used for each rat for power spectral analyses. Herein, SWA, infraslow SWA, and infraslow SWA phase within each NREM episode were calculated as described above. For each putative excitatory or inhibitory neuron, firing rate data were transformed into spike counts during nonoverlapping 4-s bins. Within each NREM episode, spike counts were normalized for each neuron as a percent of that neuron's mean firing rate across that NREM episode. Normalized firing rates were filtered in the infraslow range and instantaneous phase calculated for each neuron's firing rate across each NREM episode. Instantaneous phase differences between these filtered, normalized firing rates and infraslow SWA were calculated as described above. To test the stability of these phase differences across time, a Rayleigh test for uniformity was performed using each neuron's calculated phase differences across the entirety of the recording period. Deviations from uniformity ($p < 0.05$) reflect stability of observed phase differences. Across the entire population of neurons, an Omnibus test for circular uniformity was applied to average phase differences as these data appeared bimodal and therefore do not meet the assumptions of the Rayleigh test. To assess the relationships between neuronal firing rates and infraslow SWA across all episodes and all rats, infraslow SWA was again divided into eight nonoverlapping phase bins. Average SWA and firing rates were calculated within each bin, averaged across all NREM episodes, and then averaged across the 10 rats.

"On" and "Off" periods and transition synchrony.

During NREM sleep, cortical neurons exhibit a characteristic firing pattern consisting of alternations between "On" periods (brief periods of widespread neuronal activity) and "Off" periods (brief periods of neuronal silence). "On" and "Off" periods in this

data set were previously detected [31] by largely following an earlier methodology [11]. Briefly, "Off" periods were characterized as short (75–1,250 ms) periods of population-wide silence. "On" periods were defined as population firing (at least 10 total spikes, 200–4,000 ms duration) occurring between "Off" periods. Transition synchrony was defined in a manner similar to that previously described [11]. Briefly, the latency from the last action potential fired for each neuron prior to an "Off" period ("On"–"Off" synchrony) or immediately following the cessation of an "Off" period ("Off"–"On" synchrony) was calculated. As these analyses were focused on neuronal activity immediately surrounding these transitions, spike latencies exceeded 50 ms were excluded. Transition synchrony was then defined as 1/(latency standard deviation). For comparisons with infraslow SWA, average "On" and "Off" period durations and transition synchrony values were calculated in nonoverlapping 4-s bins across each NREM episode as described above. To assess whether transition synchrony was associated with infraslow SWA, two complementary approaches were then undertaken: (1) average transition synchrony was calculated within eight phase bins across the infraslow cycle and a repeated measures ANOVA was used to determine whether phase significantly affected synchrony and (2) the average transition synchrony values were correlated with SWA. A similar methodological approach was taken to assess whether the number of "On" and "Off" periods varied in association with infraslow SWA.

Statistical approaches.

Similar statistical approaches were taken for both data sets. Repeated measures ANOVAs, correlations, and linear regressions were performed with SPSS (IBM, Armonk, NY). Circular statistics (i.e. circular mean tests, Watson-Williams tests, and circular-linear correlations) were performed in Matlab with the CircStat toolbox [34]. All linear data are presented as mean ± the standard error of the mean. All circular data are presented as the circular mean ± the standard error of the mean. Statistical significance was assessed at $p < 0.05$.

Results

Cortical SWA is homeostatically regulated across the light period

SWA (the EEG/LFP power between 0.5 and 4 Hz during NREM sleep) is the best electrophysiological marker of homeostatic sleep need [1]. In Sprague-Dawley rats ($N = 7$), we observed a canonical decline in SWA across the light period in both the right motor cortex LFP and the contralateral parietal EEG (main effect of time, $F(11,66) = 6.71$, $p < 0.001$; no significant effects of recording site, $F(1,6) = 1.48$, $p = 0.27$, or interaction, $F(11,66) = 0.45$, $p = 0.93$; Figure 1A). Consistent with previous reports [9, 10, 12], this homeostatic decline in SWA was associated with a significant reduction in individual slow wave amplitude ($F(2,12) = 63.01$, $p < 0.001$), ascending slope ($F(2,12) = 62.18$, $p < 0.001$), and a significant increase in the proportion of multipeak slow waves ($F(2,12) = 9.69$, $p < 0.01$; see Figure 1B). Thus, as sleep need dissipates the aggregate characteristics of individual slow waves and SWA are predictably modulated.

Cortical SWA is additionally regulated across infraslow timescales

Although average hourly values of SWA reliably reflect sleep need, the generation of SWA is a dynamic process that exhibits extensive variability across shorter timescales (i.e.

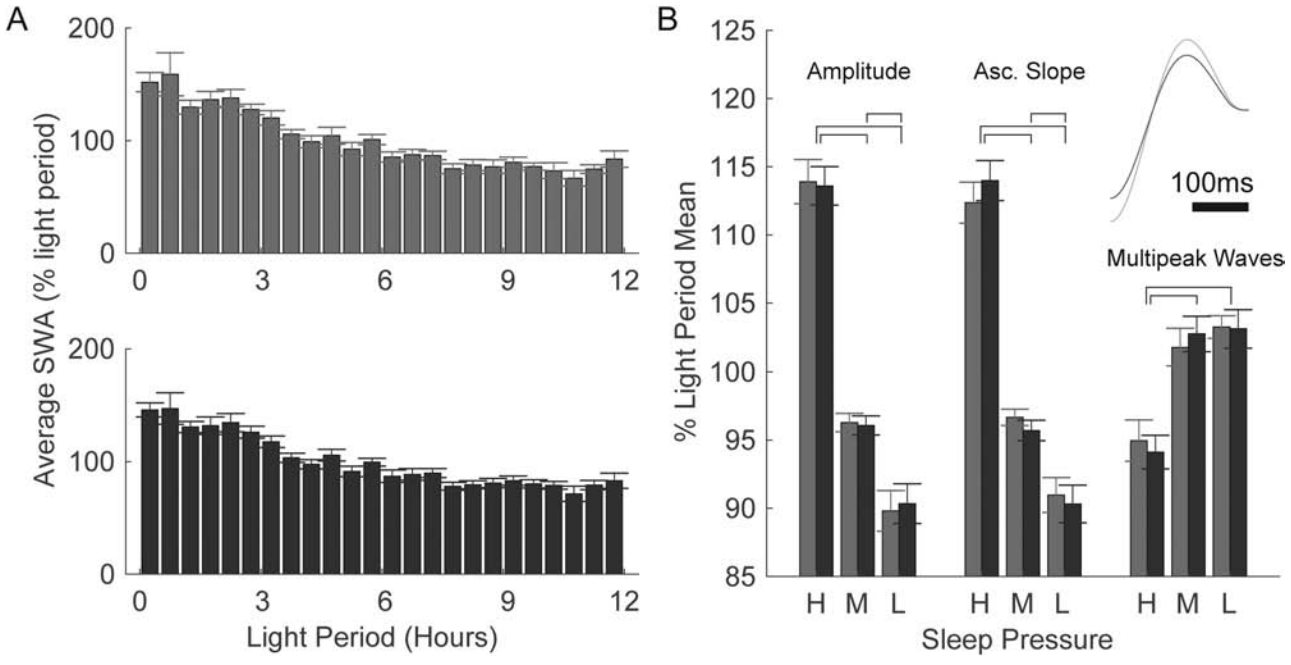

Figure 1. Homeostatic sleep need reliably regulates SWA and individual slow wave characteristics. (A) Average SWA across the light period in the motor cortex (gray) and parietal cortex (black). (B) Changes in motor cortex (gray) and parietal cortex (black) individual slow wave amplitude, ascending slope, and proportion of multipeak waves as a function of sleep pressure (High: first 3 h of light period; Medium: hours 4.5–7.5, and Low: last 3 h of light period). Brackets depict significant differences ($p < 0.05$) from post hoc analyses of the significant main effect of sleep pressure. Inset depicts the average slow wave observed under high (gray) and low (black) sleep pressure.

seconds to minutes). For example, the average standard deviation of SWA during each consolidated NREM episode was 83.15 ± 1.24% and 83.73 ± 1.25% of the total standard deviation observed across the entire light period for the RFLFP and LPEEG, respectively. To identify and characterize potential sources of this variability, we examined SWA within each consolidated NREM episode (see Figure 2A for an individual example). Fluctuations in SWA within NREM episodes do not appear to be fully stochastic and instead appear to exhibit spontaneous fluctuations across infraslow timescales (i.e. ~40- to 120-s periods). Consequently, SWA was filtered in the infraslow range and the instantaneous phase of this infraslow activity was calculated (Figure 2A). On average, infraslow phase alone explained 15.08 ± 1.67% of SWA variability within NREM episodes. To further identify the extent to which infraslow activity modulates SWA, for each rat recorded, linear regressions with infraslow phase and light-period time as predictors of SWA were performed (see Figure 2B for an individual example and Figure 2C for regression outputs). Including infraslow phase in addition to time of day significantly improved the regression model fit for every rat (*F*-change statistic; all p's < 0.01), and in every regression the coefficients for both predictors (i.e. infraslow phase and time of day) were statistically significant (*t*-scores; all p's < 0.01). On average, including these two predictors explained 26.0 ± 2.0% of total SWA variance. Thus, both time of day and infraslow phase appear to be significant sources of SWA variability.

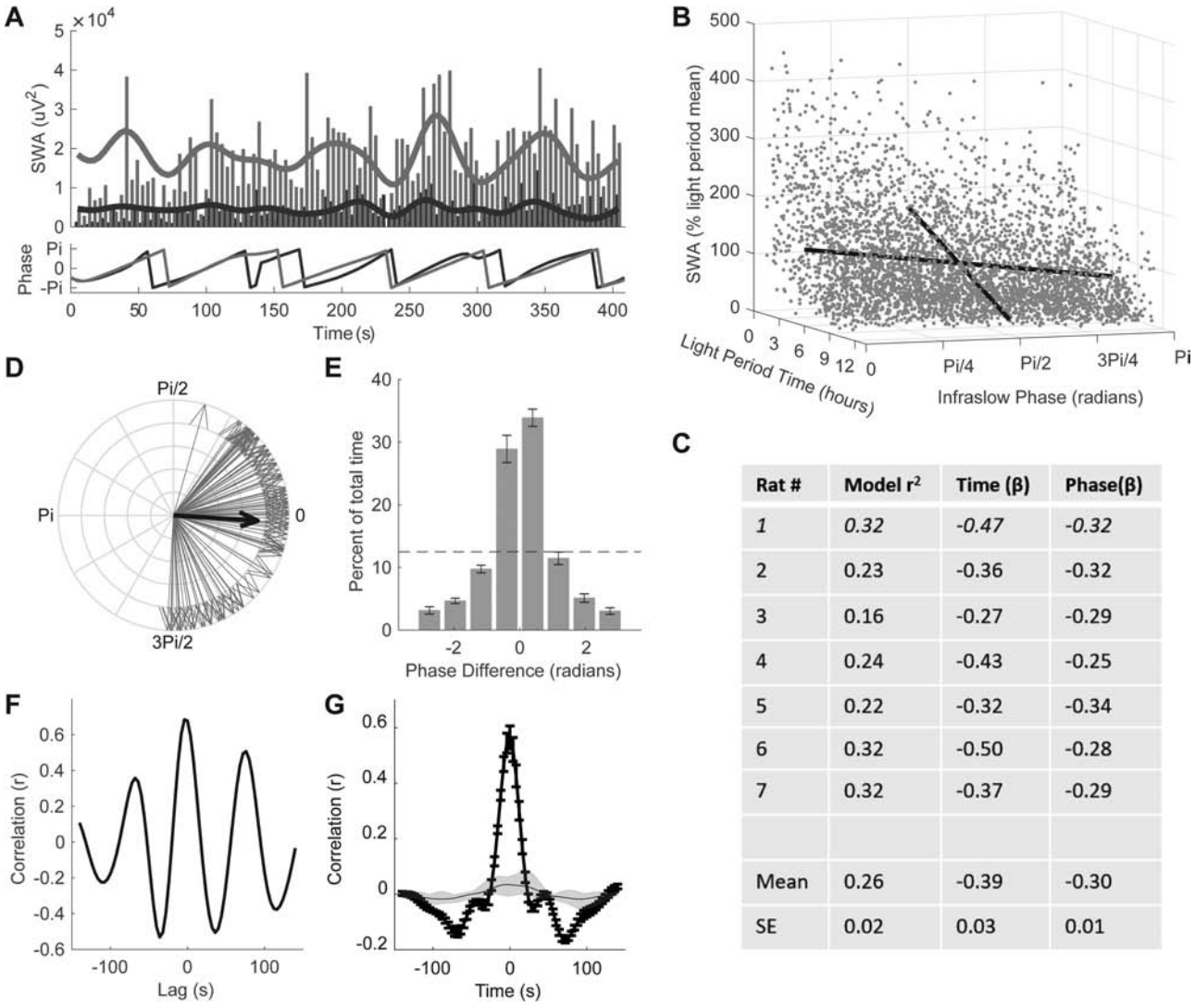

Rat #	Model r²	Time (β)	Phase(β)
1	*0.32*	*-0.47*	*-0.32*
2	0.23	-0.36	-0.32
3	0.16	-0.27	-0.29
4	0.24	-0.43	-0.25
5	0.22	-0.32	-0.34
6	0.32	-0.50	-0.28
7	0.32	-0.37	-0.29
Mean	0.26	-0.39	-0.30
SE	0.02	0.03	0.01

Figure 2. Infraslow oscillations coordinate and modulate SWA. (A) Top panel: SWA within the right motor cortex (gray) and left parietal cortex (black) is depicted for each 4-s epoch of a consolidated NREM episode; overlay depicts filtered infraslow SWA traces. Bottom panel: instantaneous phase of infraslow SWA recorded from each cortical location. (B) SWA from all 4-s NREM epochs during the light period in a single rat as a function of the absolute value of infraslow phase and light-period time (from light onset, t = 0 to light offset, t = 12). Black lines depict the best-fit line for each predictor. Model results from this regression (Rat # 1) and those from all other rats are presented in C. (D) Average phase difference (black vector) and instantaneous phase differences (gray vectors, each 4-s epoch) between infraslow SWA in the motor and parietal cortex during the NREM episode depicted in A. (E) Average phase difference observed during all NREM episodes from all rats. Infraslow SWA is typically in-phase between motor cortex and parietal electrodes. Dashed line depicts expected phase differences by chance alone. (F) Cross-correlation between motor and parietal cortex infraslow SWA during the episode depicted in A. (G) Average cross-correlation between motor and parietal cortex infraslow across all rats and all NREM episodes (black). Gray tracing depicts a 95% confidence interval derived from shuffled data (see Methods section).

Infraslow activity coordinates SWA between cortical regions

Infraslow fluctuations can coordinate neuronal activity between spatially segregated brain regions [27–29] and therefore may coordinate the expression of SWA throughout the cortex. To test this possibility, we used two complementary approaches to examine whether infraslow activity is coordinated between the right motor cortex LFP and contralateral parietal EEG. In the first approach, instantaneous infraslow phase was calculated within each brain region and instantaneous phase differences were derived by comparing those signals. Figures 2A and 2D depict the results of these analyses for a single NREM episode; during this episode, infraslow SWA was consistently in-phase between these cortical regions. Across all rats and NREM episodes, significant phase locking was observed between the right motor and left parietal cortices ($F(7,42) = 95.95$, $p < 0.01$; Figure 2E) with an average instantaneous phase difference that was not statistically significant from zero (circular mean ± circular standard deviation: 0.08 ± 0.10 radians; circular mean test: $p > 0.05$).

For our second approach, we calculated the cross-correlation of infraslow SWA from each cortical region for each consolidated NREM episode. Cross-correlations from individual NREM episodes consistently exhibited high positive correlations with zero lag as well as a clear rhythmicity within infraslow timescales (see Figure 2F for an individual example). Across all animals and NREM episodes, the cross-correlation revealed high levels of synchrony around zero lag (average Pearson's r: 0.57 ± 0.04; Figure 2G). Notably, unlike in examples from individual NREM episodes, clear infraslow rhythmicity was not observed across the total population, likely because of the nonharmonic characteristic of infraslow fluctuations [28]. Collectively, however, the significant phase locking and cross-correlations described above indicate that infraslow fluctuations can serve to coordinate SWA across disparate cortical locations.

Given the clear coordination of infraslow SWA between cortical regions described above, we further explored how infraslow activity affects SWA by examining the characteristics of individual slow waves across the infraslow cycle. We first subdivided infraslow SWA recorded within the right motor cortex into eight phase bins (similar results were observed if left parietal infraslow activity was used instead, data not shown). Individual slow waves that occurred within each phase bin were then averaged to identify how infraslow phase affects slow wave characteristics (Figure 3A). Infraslow SWA phase significantly affected individual slow wave amplitude ($F(7,42) = 87.24$, $p < 0.001$), ascending slow wave slope ($F(7,42) = 87.13$, $p < 0.001$), and wave duration ($F(7,42) = 5.30$, $p < 0.001$), with peaks in infraslow SWA associated with increases in each of these characteristics. Infraslow SWA phase also significantly affected the total number of slow waves observed ($F(7,42) = 5.61$, $p < 0.001$) and the proportion of multipeak waves ($F(7,42) = 15.03$, $p < 0.001$), with peaks in infraslow SWA associated with fewer total waves and smaller proportion of multipeak waves observed. Thus, peaks in SWA across infraslow timescales appear to be arise from large, long-duration, single-peak slow waves as opposed to a general increase in the number of waves generated.

Infraslow variation in SWA is associated with altered neuronal synchrony

To identify physiological mechanisms that contribute to the generation of infraslow SWA, we turned to a freely available online data set [30] which contains coupled recordings of neuronal firing and LFP activity across periods of consolidated sleep in male Long-Evans rats. Similar to the data described above, the phase of infraslow SWA from this second data set strongly modulated characteristics of individual slow waves (Figure 3B). Peaks in infraslow SWA were associated with significant increases in the amplitude ($F(7,63) = 23.59$, $p < 0.001$), ascending slope ($F(7,63) = 23.40$, $p < 0.001$), and duration ($F(7,63) = 5.55$, $p < 0.001$) of slow waves. Meanwhile, significant decreases in the total number of waves ($F(7,63) = 2.75$, $p < 0.05$) and the proportion of multipeak waves ($F(7,63) = 2.67$, $p < 0.05$) were observed in association with peak infraslow SWA. Thus, infraslow SWA is present within both Sprague-Dawley and Long-Evans rats and appears to arise from similar alterations to the characteristics of individual slow waves within each rat strain.

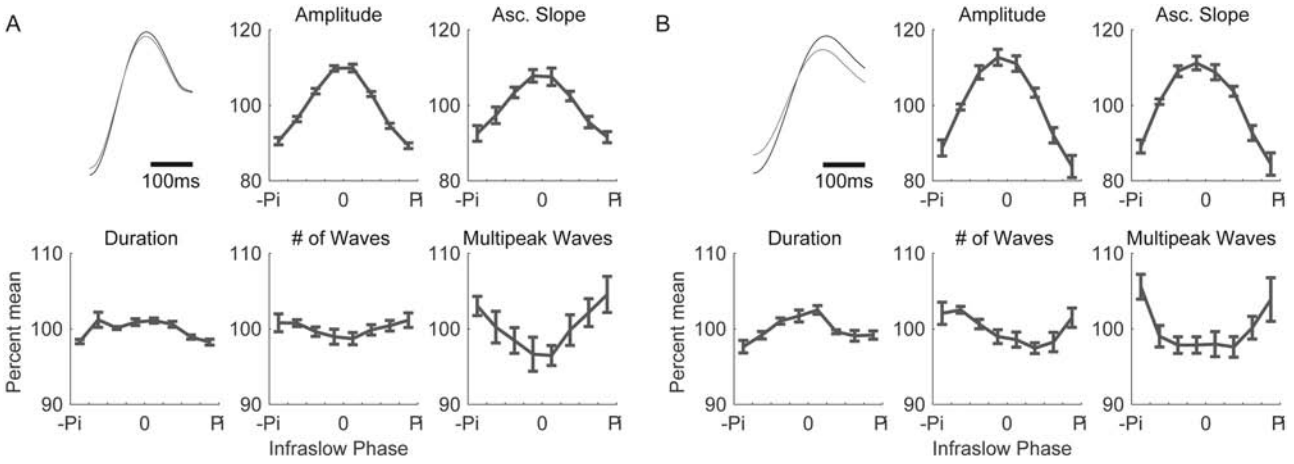

Figure 3. Infraslow SWA oscillations modulate individual slow wave characteristics. (A) Individual slow wave data from the right motor cortex of seven Sprague-Dawley rats. (B) Individual slow wave data from frontal cortical regions of 10 Long-Evans rats. Upper left panels in A/B depict average slow wave waveforms during infraslow SWA peaks (infraslow phase range: –Pi/4 to Pi/4; black lines) and infraslow SWA nadirs (infraslow phase ranges: –Pi to –3Pi/4 and 3Pi/4 to Pi; gray lines). The remaining panels in A/B depict how infraslow SWA phase affects the average characteristics of individual slow waves including wave amplitude, ascending slope, wave duration, total number of waves observed, and the proportion of multipeak waves observed.

As SWA and individual slow waves arise from underlying patterns and levels of neuronal firing, we explored whether the firing activity of putative excitatory and inhibitory neurons was associated with infraslow SWA. Within each consolidated NREM sleep episode, spike counts for each neuron were calculated across 4-s epochs. Spike counts for each neuron were then normalized to the mean firing rate of that neuron across the NREM episode. As evident in Figure 4A, the firing rates of both excitatory and inhibitory neurons typically change in association with infraslow SWA phase; individual neurons, however,

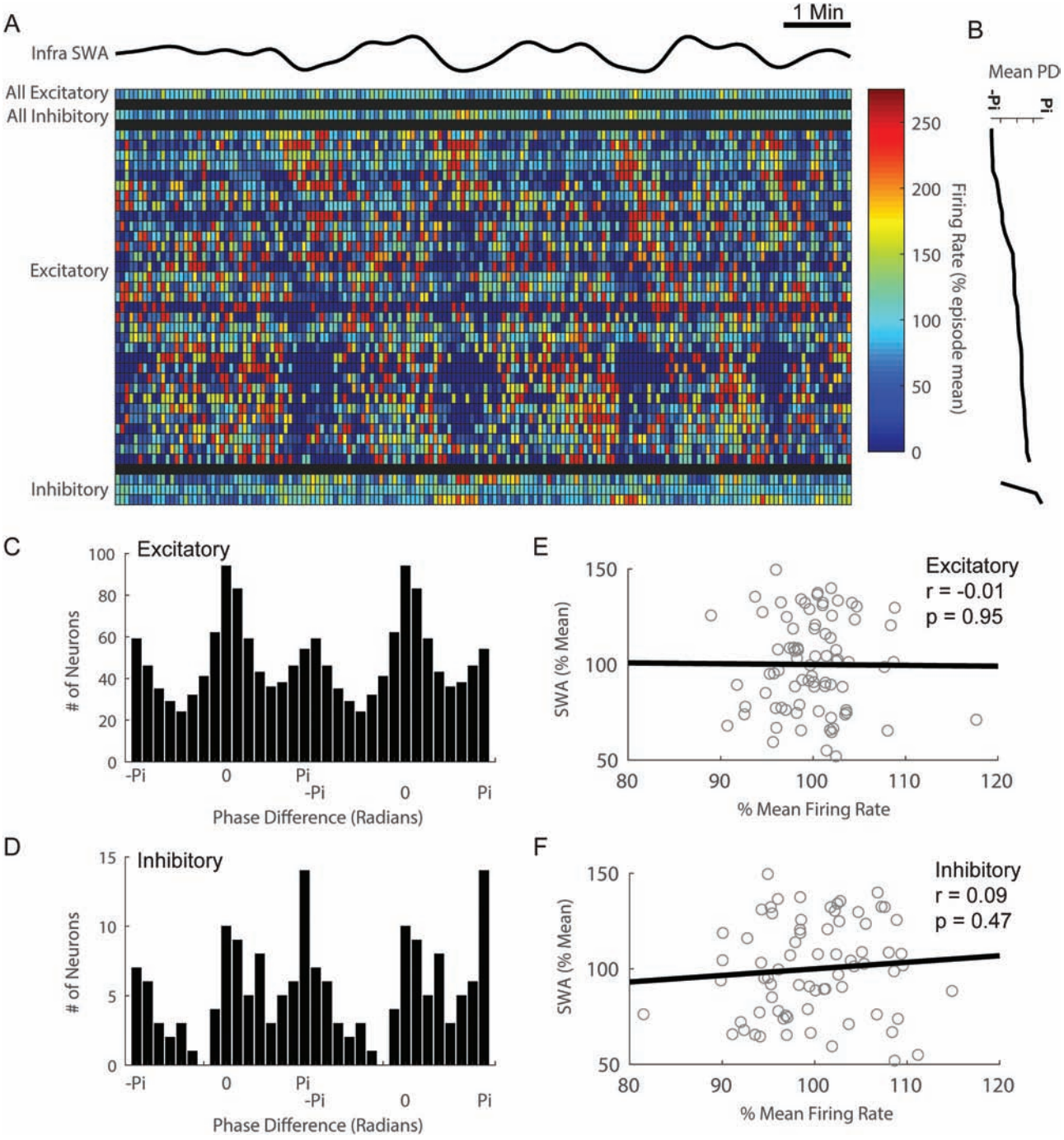

Figure 4. Infraslow SWA is not correlated with excitatory or inhibitory firing rates. (A) Top trace: infraslow SWA across a consolidated NREM episode. Heatmap: firing rates (normalized to the mean firing rate of this NREM episode for each neuron) for each putative excitatory and inhibitory neuron are depicted as separate rows in 4-s bins across the NREM episode. Composite excitatory and inhibitory firing rates are also depicted. Excitatory and inhibitory neurons have been sorted by their average phase difference with the infraslow SWA to better visualize the observed heterogeneity of phase differences. To limit the effect of outliers on the heatmap visualization, all firing rats >300% of the episode mean are plotted as equal to 300%. (B) Average phase differences between infraslow SWA and each individual neuron that is depicted in A. (C/D) Histogram of observed phase differences between infraslow SWA and excitatory (C) or inhibitory neurons (D). Data are double-plotted to better visualize the bimodal distribution of phase differences. (E/F) Across all NREM episodes and all rats, neither the mean firing rates of excitatory (E) nor inhibitory neurons (F) were significantly correlated with SWA across the infraslow cycle.

exhibit widespread heterogeneity in regards to how their firing rates changes relative to the infraslow SWA cycle. As evident from the instantaneous phase differences (PD) between infraslow SWA and the firing rates of each individual neuron (Figure 4B), some neurons exhibit peak firing in association with peak infraslow SWA (mean PD = 0), others exhibit peak firing during infraslow SWA nadirs (mean PD = –Pi/Pi), while others exhibit peak firing between these extremes. Despite this heterogeneity, phase differences between individual neurons' firing rates and infraslow SWA across all rats were not uniform for excitatory or inhibitory neurons (Omnibus test for circular uniformity [34], both p's < 0.001). Instead, bimodal phase differences were observed for both excitatory and inhibitory neurons with more neurons exhibiting peak firing rates around either infraslow SWA peaks or nadirs (Figure 4C/D). Phase differences for the majority of individual neurons appear to be stable across the recording session; 85.31% of neurons exhibited instantaneous phase distributions derived across all consolidated NREM episodes that significantly deviate from uniform as assessed by the Rayleigh test for nonuniformity. Thus, while the firing rates of individual neurons exhibit heterogeneous phase differences with respect to ongoing infraslow SWA, these phase differences appear largely stable across time. The underlying mechanism for this observed heterogeneity remains unclear as neither cortical region (Watson-Williams test [34]: $F(3,828) = 1.73$, $p = 0.16$), average firing rate (circular-linear correlation [34]: $c = 0.02$, $p = 0.82$), nor putative cell type (i.e. excitatory/inhibitory; Watson-Williams test: $F(1,830) = 0.76$, $p = 0.38$) significantly accounted for observed phase differences.

To further explore the relationships between firing rate and infraslow SWA at a population level, we first subdivided the infraslow SWA cycle into eight phase bins. For each rat, normalized, mean firing rates for putative excitatory or inhibitory neurons across all NREM episodes were averaged within each phase bin. Average SWA was likewise calculated within each phase bin. Neither excitatory ($r = –0.01$, $p = 0.95$; Figure 4E) nor inhibitory ($r = 0.09$, $p = 0.47$; Figure 4F) firing rates were correlated with SWA across infraslow cycles. Thus, although the firing rate of many neurons appears to be modulated across infraslow timescales, the relationship of these firing rates to infraslow SWA is highly variable. Infraslow SWA does not appear, therefore, to arise from consistent alterations in population firing rates.

Alternating periods of neuronal silence ("Off" periods) and neuronal firing ("On" periods) underlie sleep, slow waves (Figure 5A). Previous reports have indicated that homeostatic alterations in SWA are associated with changes in neuronal synchrony during transitions between "On" and "Off" periods [11]. Similar changes in synchrony could contribute to the observed infraslow SWA variability observed in the present study. Consequently, we calculated indices of neuronal synchrony surrounding transitions from "On" to "Off" states, and vice versa. Unlike the firing rate modulation described above, transition synchrony was reliably modulated across the infraslow cycle ("On"–"Off" transitions: $F(7,63) = 3.89$, $p < 0.01$; "Off"–"On" transitions: $F(7,63) = 4.30$, $p < 0.01$; Figure 5B). Across infraslow cycles, SWA was significantly correlated with transition synchrony ("On"–"Off" synchrony: $r = 0.47$, $p < 0.001$, "Off"–"On" synchrony: $r = 0.39$, $p < 0.001$; Figure 5C). Together, these results appear to indicate that enhanced neuronal recruitment (i.e. from "Off" to "On" periods) and decruitment (i.e. from "On" to "Off" periods) contribute to infraslow variations in SWA.

Changes in the efficacy of recruitment/decruitment could further influence SWA by altering the duration and/or number of "On" and/or "Off" periods. Similar to the changes in neuronal synchrony described above, the number $F(7,63) = 13.21$, $p < 0.001$) and duration ($F(7,63) = 5.34$, $p < 0.001$) of "Off" periods were significantly modulated across the infraslow SWA cycle; increases in SWA across the infraslow cycle were associated with more frequent and longer "Off" periods (Figure 5D). Consistent with this observation, SWA across the infraslow cycle was significantly correlated with both the number ($r = 0.79$, $p < 0.001$) and duration ($r = 0.66$, $p < 0.001$) of "Off" periods (Figure 5E). Although the number of "On" periods was similarly modulated across the infraslow SWA cycle ($F(7,63) = 9.24$, $p < 0.001$), we did not observe a significant effect of infraslow SWA cycle on "On" period duration ($F(7,63) = 1.44$, $p = 0.21$). Thus, changes in the number of "On"/"Off" periods, "Off" period duration, and transition synchrony are associated with infraslow SWA.

Infraslow modulation extends beyond sleep SWA

Previous reports indicate that infraslow activity can modulate EEG power across a wide range of higher frequencies during both sleep and wake [23, 26, 35]. We therefore examined whether the infraslow alterations in SWA documented above were additionally associated with changes in EEG power within other frequency bands (see Methods section for detailed explanation). Across infraslow cycles, SWA was significantly correlated with both theta and alpha power ($r(110) = 0.90$, $p < 0.01$ and $r(110) = 0.32$, $p < 0.05$, respectively) but not with power in other frequency bands (low_beta: $p = 0.80$, high_beta: $p = 0.74$, low_gamma: $p = 0.15$, high_gamma: $p = 0.61$). Using a similar approach, we further investigated whether higher frequency power was also modulated by infraslow activity during consolidated waking bouts. Strikingly, waking infraslow activity in the delta range (0.5–4 Hz, the same frequency range used to calculate SWA during NREM sleep) was significantly correlated with infraslow activity across all of the higher frequency bands investigated (theta: $r = 0.89$, alpha: $r = 0.60$, low_beta: $r = 0.80$, high_beta: $r = 0.69$, low_gamma: $r = 0.88$, and high_gamma: $r = 0.78$; all $df = 110$, all $p < 0.01$). Thus, similar to previous reports [23, 26, 35], infraslow fluctuations observed in the present study contribute to significant nesting of higher frequency power across multiple frequency bands. While significant nesting persists during NREM sleep, it appears to only do so within relatively lower frequencies (delta, alpha, and theta).

Discussion

The expression of cortical SWA is homeostatically regulated with a well-characterized decline across prolonged periods of sleep. We observe that SWA is additionally regulated across shorter timescales; extensive infraslow SWA fluctuations (<0.1 Hz) are present within each NREM episode and contribute to intra-episode SWA variability that is ~80%–85% of that observed across the typical homeostatic decline. Infraslow SWA fluctuations were typically in-phase between the right motor and left parietal cortices and thereby appear to coordinate SWA across disparate cortical locations. Peak SWA across the infraslow cycle was associated with increased amplitude, slope, and duration of individual slow waves with a concurrent

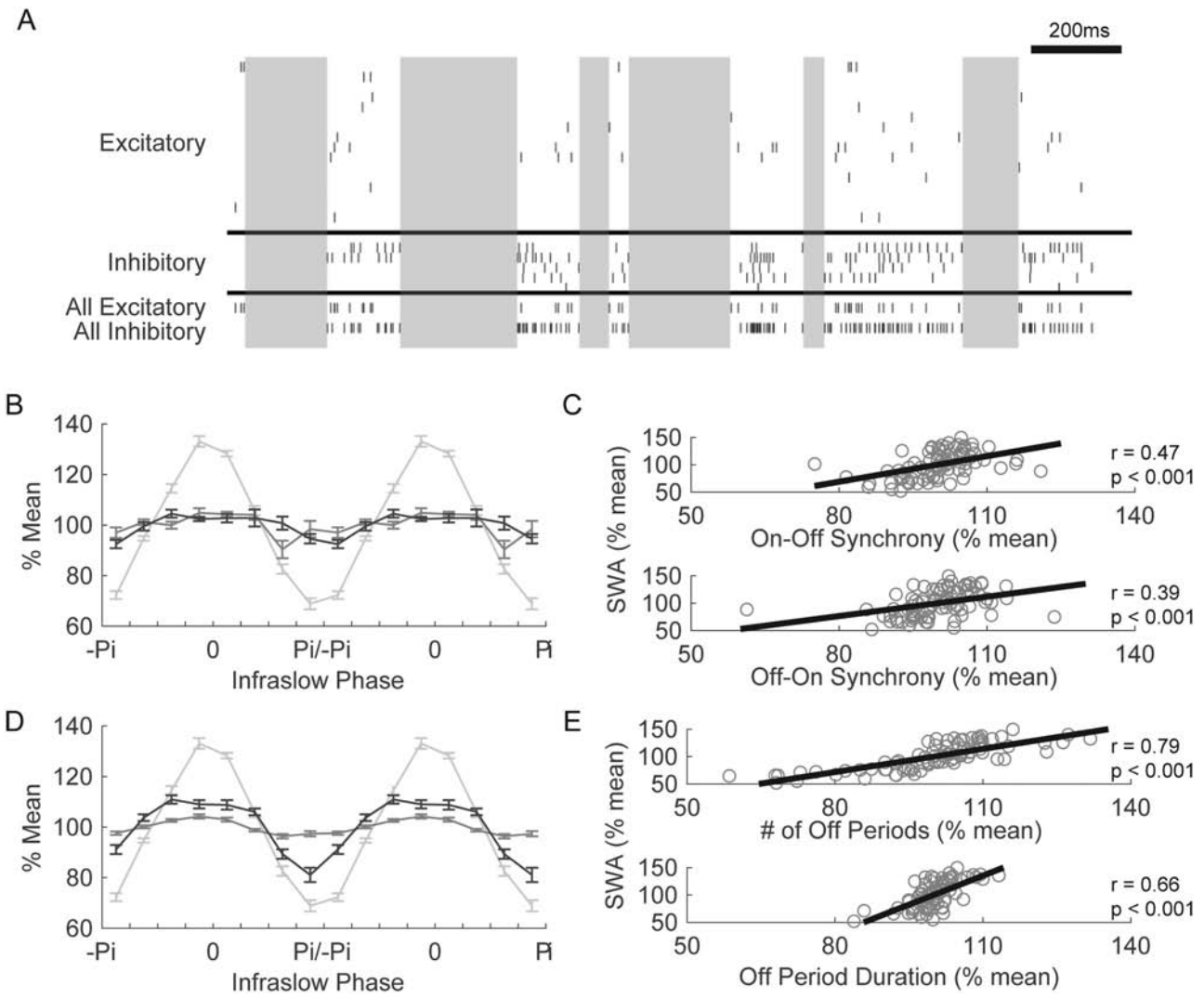

Figure 5. Infraslow SWA is associated with changes in neuronal synchrony and the number and duration of off periods. (A) A raster plot of putative excitatory and inhibitory firing across "On" and "Off" periods (white and gray, respectively). Each row represents an individual neuron and each vertical tick an action potential. Composite excitatory and inhibitory firing are also depicted. (B) Average SWA (light gray), neuronal synchrony during transitions to "Off" periods from "On" periods (gray), and neuronal synchrony during transitions to "On" periods from "Off" periods (black) are depicted as a function of the infraslow SWA cycle. (C) Neuronal synchrony is significantly correlated with SWA across the infraslow cycle. (D) Average SWA (light gray), "Off" period duration (gray), and number of "Off" periods (black) are depicted as a function of the infraslow SWA cycle. (E) The number and duration of "Off" periods are significantly correlated with SWA across the infraslow cycle. B/D are each double-plotted to better visualize infraslow rhythmicity.

decrease in the number of slow waves and proportion of multipeak waves. SWA peaks were additionally associated with increased neuronal synchrony surrounding transitions between "On" and "Off" periods and more frequent and longer "Off" period durations. By contrast, firing rates of putative excitatory or inhibitory neurons were not significantly associated with infraslow SWA variability. Through characterizing the coordination and control of SWA expression, we can better understand how this neuronal activity directly contributes to sleep function.

The function of sleep, and by association the physiological role of SWA, remains unclear. A growing consensus [36–41], however, suggests that SWA is important for the regulation of memory and corresponding synaptic plasticity. Indeed, enhancing SWA through electrical [3] or auditory [4, 42] stimulation produces marked improvements in memory while selective SWA deprivation impairs memory [2, 43]. Two primary mechanisms have been proposed to account for SWA-dependent memory improvement: (1) the selective strengthening and consolidation of specific memory traces [44–47] and (2) nonselective reductions in global synaptic strength that could improve signal-to-noise ratio within cortical networks [48–50]. Recent evidence may provide a basis to integrate these otherwise contrasting roles; SWA may broadly downscale synaptic strength while maintaining and/or consolidating synaptic strength of specific memory traces [24, 25, 51–53]. Herein, the depolarized "Up" state of the slow wave promotes synaptic weakening unless concurrent suprathreshold postsynaptic spiking activity is present [24, 25]. Memory replay during SWA, therefore, may preserve synaptic weight within active neuronal circuits while enabling widespread reductions in synaptic strength elsewhere [51–53]. Such a mechanism could underlie selective memory facilitation observed when memory-specific odor [54] or auditory cues [55] are delivered during slow wave sleep. Understanding

the spatiotemporal expression of SWA, therefore, appears critical for understanding its role in shaping cortical plasticity.

We observe that SWA exhibits extensive intra-episode variability that is coordinated between the right motor and left parietal cortices across infraslow timescales. During waking, correlated infraslow fluctuations in resting state fMRI activity form the basis for a diverse array of functional networks [56–58]. Although similar network connectivity across infraslow timescales appears to be maintained during light sleep [59], sleep can induce robust alterations to this network communication [60, 61]. Consistent, in-phase infraslow SWA between heterotypic, contralateral recording sites in the present study further demonstrates the ability of these fluctuations to coordinate activity across the cortex. This coordination could facilitate the highly correlated expression of slow waves across cortical hemispheres [29].

Although the underlying mechanisms responsible for the generation of infraslow activity are still being characterized, these slow fluctuations have been associated with changes in brain metabolism [62] and widespread alterations in neuronal excitability [27, 63]. Astrocytic adenosine has been proposed to contribute to infraslow activity as (1) infraslow fluctuations appear dependent upon the activation of A1 receptors by adenosine [62], (2) astrocytic syncytia exhibit coordinated changes in intracellular calcium signaling across large spatial scales that fluctuate across infraslow timescales [64, 65], and (3) calcium-dependent gliotransmission can modulate neuronal activity through A1 receptors [66–68]. Infraslow alterations in adenosine could contribute to fluctuations in infraslow SWA and neuronal synchrony observed in the present study. Astrocytic calcium transients and adenosine play causal roles in the generation of the cortical slow oscillation underlying NREM SWA [67, 69]. Indeed, electrically stimulating astrocytes increases the frequency of neuronal Up states while blocking astrocytic calcium or A1 receptors decreases Up state frequency [70]. Thus, in addition to playing a causal role in the homeostatic regulation of cortical SWA [71, 72], astrocytic adenosine may additionally regulate SWA across infraslow cycles.

Infraslow activity has also been shown to modulate neuronal excitability including alterations in higher frequency EEG/LFP power [22, 23, 26, 35], cortical interictal events in epileptic patients [23], and spontaneous hippocampal afterdischarges in Wistar rats [73]. In the present study, we replicate previous findings [23, 26, 35] that demonstrate significant nesting of higher frequency BLP (0.5–80 Hz) across infraslow cycles during waking. Moreover, we show that significant reorganization of these associations occurs during NREM sleep with infraslow activity at higher frequencies (>16 Hz) no longer correlating with lower frequency activity (0.5–14 Hz). Although the functional significance of this reorganization remains to be elucidated, sleep-associated reorganization of infraslow propagation has previously been proposed to contribute to sleep function, thalamic gating, and/or sleep-associated alterations in consciousness [74].

We further observe that infraslow fluctuations alter the characteristics of spontaneous slow waves, with infraslow SWA nadirs associated with decreased slope, amplitude, and duration of individual slow waves and an increased proportion of multipeak waves. Strikingly, these changes parallel homeostatic alterations in slow wave characteristics [10] (and see Figure 1B) thought to arise as a consequence of persistent reductions in synaptic strength [9, 10, 49]. While similar changes in structural connectivity are unlikely to account for changes in slow waves across infraslow cycles, infraslow activity is dependent upon synaptic transmission (e.g. attenuated by antagonists of voltage-gated sodium channels or glutamate receptors [27]). Consequently, changes in functional connectivity that alter synaptic efficacy across infraslow timescales could account for the similarity with homeostatic slow wave modulation. Consistent with this idea, coupling between electrically evoked postsynaptic excitatory potentials and action potential generation has been shown to vary across infraslow cycles [33].

To further understand the physiological underpinnings of infraslow SWA, we examined how neuronal firing rates and patterns vary across the infraslow cycle. During spontaneous sleep across the major sleep phase, firing rates during "On" periods are significantly correlated with SWA [11], with average population firing rates declining over periods of sleep [11, 31]. However, elevated firing per se, does not appear to cause increased SWA; optogenetic stimulation to increase firing rates during NREM sleep was associated with reductions in SWA [75]. Moreover, NREM sleep bidirectionally regulates firing rates of individual neurons by increasing/decreasing firing rates in neurons with low/high basal firing levels, respectively [31]. Consistent with these results, we observed that neither the average firing rates of putative excitatory nor inhibitory neurons were correlated with SWA across infraslow cycles. This absence of significant correlation may arise from extensive heterogeneity in the phase relationship between an individual neuron's firing rate and infraslow SWA (Figure 4A/B). Across our population of neurons (Figure 4C/D), firing rates exhibited a bimodal distribution with elevated firing rates predominantly occurring around the peaks and nadirs of infraslow SWA. A strikingly similar relationship between individual neuronal firing rates and population activity has recently been described in the medial prefrontal cortex of freely behaving mice across slow timescales (<0.1 Hz) that is absent across fast timescales [76]. Firing rate phase heterogeneity, with respect to infraslow SWA, may therefore reflect an emergent organizational property of neuronal activity across slow timescales. Indeed, neither cortical location, average firing rate, nor putative cell type significantly accounted for this phase heterogeneity. Alternatively, it is intriguing to hypothesize whether this phase heterogeneity reflects the existence of multiple, distinct infraslow ensembles (e.g. [27]), though the present data set does not facilitate a direct test of this hypothesis.

Unlike firing rates, measures of neuronal synchrony and the number and duration of "Off" periods were significantly correlated with infraslow SWA. Cortical slow waves arise from alternating patterns of widespread neuronal activity and neuronal silence ("On" and "Off" periods, respectively [11, 31]). In association with the homeostatic regulation of SWA, the number and duration of "Off" periods [11, 75] decrease across prolonged periods of sleep; a similar pattern is observed for LFP "Down" states that are associated with "Off" periods [31]. Likewise, neuronal synchrony surrounding "On"/"Off" and "Off"/"On" transitions decreases across sleep [11]. These alterations appear, in part, to be driven by widespread reductions in synaptic strength [10, 50, 77]. It is unlikely that persistent changes in synaptic strength are responsible for similar changes in neuronal synchrony associated with infraslow SWA observed in the current study. Rather, as discussed above, transient changes in neuronal excitability and/or synaptic efficacy across the infraslow

cycle could account for these observations. To wit, computer simulations indicate that the synchronous termination of active firing across slow waves can be mediated by the strength of synaptic inhibition and/or the excitability of inhibitory neurons [78]. Therefore, changes in the excitability of inhibitory neurons across the infraslow cycle may provide a functional mechanism to alter synchrony surrounding "On"/"Off" transitions and thereby produce the observed infraslow fluctuations in SWA.

From "Off" period number and duration, to neuronal transition synchrony, to characteristics of individual slow waves (i.e. slope, amplitude, and proportion of multipeak waves), we observe changes across infraslow cycles that contribute to significant SWA variability. Infraslow SWA was consistently in-phase across disparate cortical regions. Consequently, infraslow fluctuations provide an important mechanism to regulate the spatiotemporal expression of SWA. Infraslow and homeostatic regulators of SWA appear to alter slow wave generation in a strikingly similar manner, albeit across vastly different timescales. Sleep spindles also appear to be regulated across both the sleep cycle [7, 79] and infraslow timescales [80] in order to balance sensory reactivity with off-line memory consolidation [80]. The precise functional significance of regulating SWA across both infraslow and homeostatic timescales, however, remains to be elucidated.

Acknowledgments

We thank the Collaborative Research in Computational Neuroscience program (CRCNS; crcns.org) for hosting the freely available data set used within this report and the authors [31] who collected the data originally.

Funding

Research reported in this publication was supported by an Institutional Development Award (IDeA) from the National Institute of General Medical Sciences of the National Institutes of Health under grant number P20GM103449. Its contents are solely the responsibility of the authors and do not necessarily represent the official views of NIGMS or NIH.
Conflict of interest statement. None declared.

References

1. Achermann P, *et al*. Mathematical models of sleep regulation. *Front Biosci*. 2003;**8**:s683–s693.
2. Landsness EC, *et al*. Sleep-dependent improvement in visuomotor learning: a causal role for slow waves. *Sleep*. 2009;**32**(10):1273–1284.
3. Marshall L, *et al*. Boosting slow oscillations during sleep potentiates memory. *Nature*. 2006;**444**(7119):610–613.
4. Ngo HV, *et al*. Auditory closed-loop stimulation of the sleep slow oscillation enhances memory. *Neuron*. 2013;**78**(3):545–553.
5. Murphy M, *et al*. Source modeling sleep slow waves. *Proc Natl Acad Sci USA*. 2009;**106**(5):1608–1613.
6. Massimini M, *et al*. The sleep slow oscillation as a traveling wave. *J Neurosci*. 2004;**24**(31):6862–6870.
7. Nir Y, *et al*. Regional slow waves and spindles in human sleep. *Neuron*. 2011;**70**(1):153–169.
8. Vyazovskiy VV, *et al*. Local sleep in awake rats. *Nature*. 2011;**472**(7344):443–447.
9. Riedner BA, *et al*. Sleep homeostasis and cortical synchronization: III. A high-density EEG study of sleep slow waves in humans. *Sleep*. 2007;**30**(12):1643–1657.
10. Vyazovskiy VV, *et al*. Sleep homeostasis and cortical synchronization: II. A local field potential study of sleep slow waves in the rat. *Sleep*. 2007;**30**(12):1631–1642.
11. Vyazovskiy VV, *et al*. Cortical firing and sleep homeostasis. *Neuron*. 2009;**63**(6):865–878.
12. Bernardi G, *et al*. Local and widespread slow waves in stable NREM sleep: evidence for distinct regulation mechanisms. *Front Hum Neurosci*. 2018;**12**:248.
13. Werth E, *et al*. Brain topography of the human sleep EEG: antero-posterior shifts of spectral power. *Neuroreport*. 1996;**8**(1):123–127.
14. Cajochen C, *et al*. Frontal predominance of a relative increase in sleep delta and theta EEG activity after sleep loss in humans. *Sleep Res Online*. 1999;**2**(3):65–69.
15. Huber R, *et al*. Local sleep and learning. *Nature*. 2004;**430**(6995):78–81.
16. Hanlon EC, *et al*. Effects of skilled training on sleep slow wave activity and cortical gene expression in the rat. *Sleep*. 2009;**32**(6):719–729.
17. Kattler H, *et al*. Effect of unilateral somatosensory stimulation prior to sleep on the sleep EEG in humans. *J Sleep Res*. 1994;**3**(3):159–164.
18. Korf EM, *et al*. Blindfolding during wakefulness causes decrease in sleep slow wave activity. *Physiol Rep*. 2017;**5**(7):e13239.
19. Huber R, *et al*. Arm immobilization causes cortical plastic changes and locally decreases sleep slow wave activity. *Nat Neurosci*. 2006;**9**(9):1169–1176.
20. Varga AW, *et al*. Effects of aging on slow-wave sleep dynamics and human spatial navigational memory consolidation. *Neurobiol Aging*. 2016;**42**:142–149.
21. Borbély AA, *et al*. The two-process model of sleep regulation: a reappraisal. *J Sleep Res*. 2016;**25**(2):131–143.
22. Liu Z, *et al*. Large-scale spontaneous fluctuations and correlations in brain electrical activity observed with magnetoencephalography. *Neuroimage*. 2010;**51**(1):102–111.
23. Vanhatalo S, *et al*. Infraslow oscillations modulate excitability and interictal epileptic activity in the human cortex during sleep. *Proc Natl Acad Sci USA*. 2004;**101**(14):5053–5057.
24. González-Rueda A, *et al*. Activity-dependent downscaling of subthreshold synaptic inputs during slow-wave-sleep-like activity in vivo. *Neuron*. 2018;**97**(6):1244–1252.e5.
25. Bartram J, *et al*. Cortical up states induce the selective weakening of subthreshold synaptic inputs. *Nat Commun*. 2017;**8**(1):665.
26. Monto S, *et al*. Very slow EEG fluctuations predict the dynamics of stimulus detection and oscillation amplitudes in humans. *J Neurosci*. 2008;**28**(33):8268–8272.
27. Chan AW, *et al*. Mesoscale infraslow spontaneous membrane potential fluctuations recapitulate high-frequency activity cortical motifs. *Nat Commun*. 2015;**6**:7738.
28. Palva JM, *et al*. Infra-slow fluctuations in electrophysiological recordings, blood-oxygenation-level-dependent signals, and psychophysical time series. *Neuroimage*. 2012;**62**(4):2201–2211.
29. Mohajerani MH, *et al*. Mirrored bilateral slow-wave cortical activity within local circuits revealed by fast bihemispheric voltage-sensitive dye imaging in anesthetized and awake mice. *J Neurosci*. 2010;**30**(10):3745–3751.

30. Watson B, *et al*. Multi-unit spiking activity recorded from rat frontal cortex (brain regions MPFC, OFC, ACC, and M2) during wake-sleep episode wherein at least 7 minutes of wake are followed by 20 minutes of sleep. *CRCNS.org*. doi:10.6080/K02N506Q
31. Watson BO, *et al*. Network homeostasis and state dynamics of neocortical sleep. *Neuron*. 2016;**90**(4):839–852.
32. Panagiotou M, *et al*. Differences in electroencephalographic non-rapid-eye movement sleep slow-wave characteristics between young and old mice. *Sci Rep*. 2017;**7**:43656.
33. Dash MB, *et al*. Spontaneous infraslow fluctuations modulate hippocampal EPSP-PS coupling. *eNeuro*. 2018;**5**(1):403–417.
34. Berens P. CircStat: a MATLAB toolbox for circular statistics. *J Stat Softw*. 2009;**31**(10):1–21.
35. Mantini D, *et al*. Electrophysiological signatures of resting state networks in the human brain. *Proc Natl Acad Sci USA*. 2007;**104**(32):13170–13175.
36. Puentes-Mestril C, *et al*. Linking network activity to synaptic plasticity during sleep: hypotheses and recent data. *Front Neural Circuits*. 2017;**11**:61.
37. Niethard N, *et al*. Plasticity during sleep is linked to specific regulation of cortical circuit activity. *Front Neural Circuits*. 2017;**11**:65.
38. Levenstein D, *et al*. Sleep regulation of the distribution of cortical firing rates. *Curr Opin Neurobiol*. 2017;**44**:34–42.
39. Timofeev I, *et al*. Sleep slow oscillation and plasticity. *Curr Opin Neurobiol*. 2017;**44**:116–126.
40. Abel T, *et al*. Sleep, plasticity and memory from molecules to whole-brain networks. *Curr Biol*. 2013;**23**(17):R774–R788.
41. Tononi G, *et al*. Sleep and synaptic down-selection. *Eur J Neurosci*. 2019;1–9. doi:10.1111/ejn.14335
42. Papalambros NA, *et al*. Acoustic enhancement of sleep slow oscillations and concomitant memory improvement in older adults. *Front Hum Neurosci*. 2017;**11**:109.
43. Aeschbach D, *et al*. A role for non-rapid-eye-movement sleep homeostasis in perceptual learning. *J Neurosci*. 2008;**28**(11):2766–2772.
44. Chauvette S, *et al*. Sleep oscillations in the thalamocortical system induce long-term neuronal plasticity. *Neuron*. 2012;**75**(6):1105–1113.
45. Aton SJ, *et al*. Mechanisms of sleep-dependent consolidation of cortical plasticity. *Neuron*. 2009;**61**(3):454–466.
46. Walker MP. The role of slow wave sleep in memory processing. *J Clin Sleep Med*. 2009;**5**(2 Suppl.):S20–S26.
47. Frank MG, *et al*. Sleep enhances plasticity in the developing visual cortex. *Neuron*. 2001;**30**(1):275–287.
48. Tononi G, *et al*. Sleep function and synaptic homeostasis. *Sleep Med Rev*. 2006;**10**(1):49–62.
49. Vyazovskiy VV, *et al*. Molecular and electrophysiological evidence for net synaptic potentiation in wake and depression in sleep. *Nat Neurosci*. 2008;**11**(2):200–208.
50. Olcese U, *et al*. Sleep and synaptic renormalization: a computational study. *J Neurophysiol*. 2010;**104**(6):3476–3493.
51. Gulati T, *et al*. Neural reactivations during sleep determine network credit assignment. *Nat Neurosci*. 2017;**20**(9):1277–1284.
52. Wei Y, *et al*. Differential roles of sleep spindles and sleep slow oscillations in memory consolidation. *PLoS Comput Biol*. 2018;**14**(7):e1006322.
53. Hashmi A, *et al*. Sleep-dependent synaptic down-selection (II): single-neuron level benefits for matching, selectivity, and specificity. *Front Neurol*. 2013;**4**:148.
54. Rasch B, *et al*. Odor cues during slow-wave sleep prompt declarative memory consolidation. *Science*. 2007;**315**(5817):1426–1429.
55. Antony JW, *et al*. Cued memory reactivation during sleep influences skill learning. *Nat Neurosci*. 2012;**15**(8):1114–1116.
56. Smith SM, *et al*. Correspondence of the brain's functional architecture during activation and rest. *Proc Natl Acad Sci USA*. 2009;**106**(31):13040–13045.
57. Karahanoğlu FI, *et al*. Transient brain activity disentangles fMRI resting-state dynamics in terms of spatially and temporally overlapping networks. *Nat Commun*. 2015;**6**:7751.
58. Biswal B, *et al*. Functional connectivity in the motor cortex of resting human brain using echo-planar MRI. *Magn Reson Med*. 1995;**34**(4):537–541.
59. Larson-Prior LJ, *et al*. Cortical network functional connectivity in the descent to sleep. *Proc Natl Acad Sci USA*. 2009;**106**(11):4489–4494.
60. Tagliazucchi E, *et al*. Decoding wakefulness levels from typical fMRI resting-state data reveals reliable drifts between wakefulness and sleep. *Neuron*. 2014;**82**(3):695–708.
61. Tagliazucchi E, *et al*. Large-scale brain functional modularity is reflected in slow electroencephalographic rhythms across the human non-rapid eye movement sleep cycle. *Neuroimage*. 2013;**70**:327–339.
62. Lörincz ML, *et al*. ATP-dependent infra-slow (<0.1 Hz) oscillations in thalamic networks. *PLoS One*. 2009;**4**(2):e4447.
63. Watson BO. Cognitive and physiologic impacts of the infraslow oscillation. *Front Syst Neurosci*. 2018;**12**:44.
64. Wang M, *et al*. Brain-state dependent astrocytic Ca2+ signals are coupled to both positive and negative BOLD-fMRI signals. *Proc Natl Acad Sci USA*. 2018;**115**(7):E1647–E1656.
65. Kuga N, *et al*. Large-scale calcium waves traveling through astrocytic networks in vivo. *J Neurosci*. 2011;**31**(7):2607–2614.
66. Parpura V, *et al*. Gliotransmission: exocytotic release from astrocytes. *Brain Res Rev*. 2010;**63**(1–2):83–92.
67. Fellin T, *et al*. Endogenous nonneuronal modulators of synaptic transmission control cortical slow oscillations in vivo. *Proc Natl Acad Sci USA*. 2009;**106**(35):15037–15042.
68. Pascual O, *et al*. Astrocytic purinergic signaling coordinates synaptic networks. *Science*. 2005;**310**(5745):113–116.
69. Szabó Z, *et al*. Extensive astrocyte synchronization advances neuronal coupling in slow wave activity in vivo. *Sci Rep*. 2017;**7**(1):6018.
70. Poskanzer KE, *et al*. Astrocytic regulation of cortical UP states. *Proc Natl Acad Sci USA*. 2011;**108**(45):18453–18458.
71. Nadjar A, *et al*. Astrocyte-derived adenosine modulates increased sleep pressure during inflammatory response. *Glia*. 2013;**61**(5):724–731.
72. Halassa MM, *et al*. Astrocytic modulation of sleep homeostasis and cognitive consequences of sleep loss. *Neuron*. 2009;**61**(2):213–219.
73. Penttonen M, *et al*. Ultra-slow oscillation (0.025 Hz) triggers hippocampal afterdischarges in Wistar rats. *Neuroscience*. 1999;**94**(3):735–743.
74. Mitra A, *et al*. Propagated infra-slow intrinsic brain activity reorganizes across wake and slow wave sleep. *eLife*. 2015;**4**:e10781. doi:10.7554/eLife.10781
75. Rodriguez AV, *et al*. Why does sleep slow-wave activity increase after extended wake? Assessing the effects of

increased cortical firing during wake and sleep. *J Neurosci*. 2016;**36**(49):12436–12447.
76. Okun M, *et al*. Distinct structure of cortical population activity on fast and infraslow timescales. *Cereb Cortex*. 2019;**29**(5):2196–2210.
77. Esser SK, *et al*. Sleep homeostasis and cortical synchronization: I. Modeling the effects of synaptic strength on sleep slow waves. *Sleep*. 2007;**30**(12):1617–1630.
78. Chen JY, *et al*. Interneuron-mediated inhibition synchronizes neuronal activity during slow oscillation. *J Physiol*. 2012;**590**(16):3987–4010.
79. Andrillon T, *et al*. Sleep spindles in humans: insights from intracranial EEG and unit recordings. *J Neurosci*. 2011;**31**(49):17821–17834.
80. Lecci S, *et al*. Coordinated infraslow neural and cardiac oscillations mark fragility and offline periods in mammalian sleep. *Sci Adv*. 2017;**3**(2):e1602026.